Phys Chem Minerals (2001) 28: 719–728

ORIGINAL PAPER

A. F. Gualtieri

Synthesis of sodium zeolites from a natural halloysite

Received: 7 November 2000 / Accepted: 19 March 2001

Abstract The kinetics of hydrothermal crystallisation of sodium zeolites from a natural mixture of halloysite and amorphous silica with Si/Al ≈ 4 was investigated. The sample collected at Scarpara (Tuscania, Italy) is the final product of an intense hydrothermal alteration process on the pre-existing leucitic tufites. In order to enhance its reactivity in the NaOH solution, the sample was thermally activated at 600 °C for 1 h. The hydrothermal crystallisation sequence of zeolites formed in the range 90–150 °C has been followed using real-time synchrotron powder diffraction. The reaction kinetics of Na-X, Na-P and analcime were analysed using a model developed for the study of the kinetic data from X-ray diffraction experiments. Na-X and Na-P cocrystallize with an autocatalytic nucleation at lower isothermal temperatures and with a heterogeneous nucleation at higher isothermal temperatures. Na-X tends to dissolve before Na-P, which in turn transforms into analcime. This work is part of a general project on the kinetics of formation of zeolites from clay precursors which is important for either engineering and production of valuable industrial materials and for the interpretation of poorly understood processes of formation of zeolites in natural hydrothermal environments.

Key words Halloysite · Kinetics of crystallisation · Sodium zeolites · Synchrotron powder diffraction

Introduction

Understanding the nucleation and growth processes of aluminosilicate zeolites (Barrer 1982; Rollman 1984) is of primary importance for either the interpretation of poorly understood processes of formation of zeolites in natural hydrothermal environments or the production of industrial materials. Clay minerals are good precursors for the synthesis. They are generally thermally activated before synthesis to increase their reactivity in solution. Given its chemical composition, kaolinite [$Al_2(OH)_4$-Si_2O_5] has been widely used with this aim in the past (Barrer et al. 1968, 1972; Madani et al. 1990).

Recently (Gualtieri et al. 1997a, b; Gualtieri and Norby 1998), we investigated the mechanism of crystallisation of zeolites formed from natural kaolinites showing a different degree of structure disorder. Samples were thermally activated at 600 and 800 °C, respectively, and used as precursors for hydrothermal synthesis using either NaOH and LiOH solutions. We found that zeolite Na-A and hydroxysodalite form using the NaOH solution in the range 70–130 °C while Li-ABW [$Li_4Al_4Si_4O_{16}{\cdot}4H_2O$] forms in the same temperature range using the LiOH solution. An autocatalytic mechanism is observed for the crystallisation of these zeolites which is independent of the degree of structural disorder of the starting kaolinite and strongly dependent on the thermal history. In fact, the crystallisation reactions are promoted by metakaolinite, the precursor activated at 600 °C. Metastable zeolite Na-A transforms into stable hydroxysodalite by an Ostwald's ripening process. In earlier experiments, the nature of the cation in solution (Na or Li) was varied while the Si:Al ratio (1:1) of the precursor was kept fixed. It is now interesting to assess the influence of a different Si:Al ratio. To form zeolites with a SiO_2/Al_2O_3 ratio >2, additional silica must be added to metakaolin. For example, to produce zeolite Na-X, a typical reaction mixture may have a composition of $4Na_2O{\cdot}Al_2O_3{\cdot}4SiO_2{\cdot}160H_2O$. The additional silica may be added in the form of sodium silicate or other sources such as colloidal silica (Breck 1974). Among the many available, a natural precursor was selected with this aim. The sample is a natural interdispersed mixture of halloysite [$Al_2(OH)_4Si_2O_5{\cdot}nH_2O$] and amorphous silica [$SiO_2{\cdot}nH_2O$] with Si/Al ≈ 4. Although the basic

A. F. Gualtieri
Dipartimento di Scienze della Terra,
Università di Modena e Reggio Emilia,
Via S.Eufemia 19, 41000 Modena Italy
Fax: +39-59-2055887
e-mail: alex@unimo.it

structure of halloysite and kaolinite is the same (a Si-tetrahedral sheet joined to an Al-octahedral sheet by sharing a plane of oxygens: (Costanzo and Giese 1985; Bailey 1988), halloysite is hydrated (halloysite-10 Å) and thus differs from kaolinite by the presence of water in the interlayer spaces. Halloysite-10 Å is unstable under ambient conditions and rapidly dehydrates (to the so-called halloysite-7 Å) if not kept in water.

In this work, the crystallisation kinetics in hydrothermal environment (NaOH solution) of the zeolites formed from halloysite thermally activated at 600 °C were analysed.

Experimental methods

Materials

The precursor of the synthesis experiments was a natural finely interdispersed mixture of 50 wt% halloysite and 50 wt% amorphous silica from Scarpara (Tuscania, Italy) (Gualtieri and Bertolani 1991a, b) with an Si/Al ratio of 4.23. This assemblage is the product of an intense hydrothermal alteration process on preexisting leucitic tufites with newly formed halloysite-10 Å and residual amorphous silica. The sample was thermally treated at 600 °C for 1 h and the product was ground in agate mortar, sieved and soaked in a 4 M NaOH solution with solidus to liquidus ratio of 0.5 in weight for the synthesis experiments.

Kinetic experiments

The solution was syringed into a 0.7-mm ϕ quartz capillary and mounted in a Swagelock device fitting with a Vespel ferrule which is set on a standard goniometer head for the data collection. The sample holder (Norby 1996) allows oscillation of the capillary in parallel-beam Debye–Scherrer transmission geometry. A pressure of about 10^6 Nm^{-2} is applied inside the capillary from an N_2 cylinder. The temperature is controlled using a stream of hot air from a heating gun positioned below the capillary and measured by a thermocouple positioned at about 1 mm below the capillary. By heating only part of the reaction mixture, evaporation is suppressed because of the low temperature of the N_2-solution boundary (Norby 1997). The reactions were followed by real-time synchrotron powder diffraction at the X7B beam line of the National Synchrotron Light Source (Brookhaven National Laboratory, USA) (Hastings et al. 1990), with a Huber four-circle diffractometer. The heated zone was ca. 5 mm, while the X-ray beam was 2 mm wide and 0.7 mm high. The width of the X-ray beam was kept much smaller than the heated zone to limit temperature gradients across the beam and to reduce problems with transport of material by convection or diffusion (Norby 1997). The experiment was performed using a fixed λ of 1.00473 Å. A 3-mm-wide cross-section of the diffracted rings was recorded on an image plate (IP) detector (Amemija 1990), mounted on a translating system called the translating image plate system (TIPS) (Norby 1996). The image plate detector is mounted on a slide behind a steel screen with a vertical 3-mm-wide slit, and the heating rate of the experiments was synchronized with the speed of the slide in order to record the continuous change of the diffracted rings with time in the isothermal runs. The images stored in the IP were recovered using a Fuji BAS2000 scanner through an He–Ne laser stimulation. Isothermal runs were performed at 90, 100, 110, 130, 140 and 150 °C. The heating rate to take the sample to the isothermal temperature was 100 °C min^{-1} for each run. Raw data, preventively corrected on site for the intensity decline vs. time of the synchrotron beam, were corrected for the zero shift error, Lorentz polarization and tilting angle of the IP. The reaction kinetics were followed by measuring the growth and development of the zeolite diffraction peaks as a function of time. Figure 1 reports the 3-D plot relative to the crystallisation of Na-P and analcime in the run at 140 °C. The phase identification is performed by comparing the observed powder patterns with the calculated ones reported in (Treacy et al. 1996). A line integration procedure was utilised for each data collection to obtain integrated areas and FWHMs (full width at half maximum) vs. time in order to follow the reaction kinetics with a good statistical meaning. The peaks utilised for the integration procedure for each zeolite phase are reported in Table 1. Reduced integrated intensities were normalised to phase fractions (or conversion factors α, the normalised amount of phase formed) and plotted as α/time curves for the three different zeolites Na-X, Na-P and analcime (Fig. 2a, b, c, respectively).

The final product of the synthesis at 130 °C with Na-P and minor analcime was used for a Rietveld structure refinement using a *CuKα* monochromatized radiation in a conventional Bragg–Brentano (BB) parafocusing geometry and the GSAS package (Larson and Von Dreele 1996). The starting atomic coordinates for the structural model were taken from (Albert et al. 1998).

SEM

Na-P formed at 130 °C was also investigated with SEM using a Philips XL40/604. Powders were mounted on an Al specimen

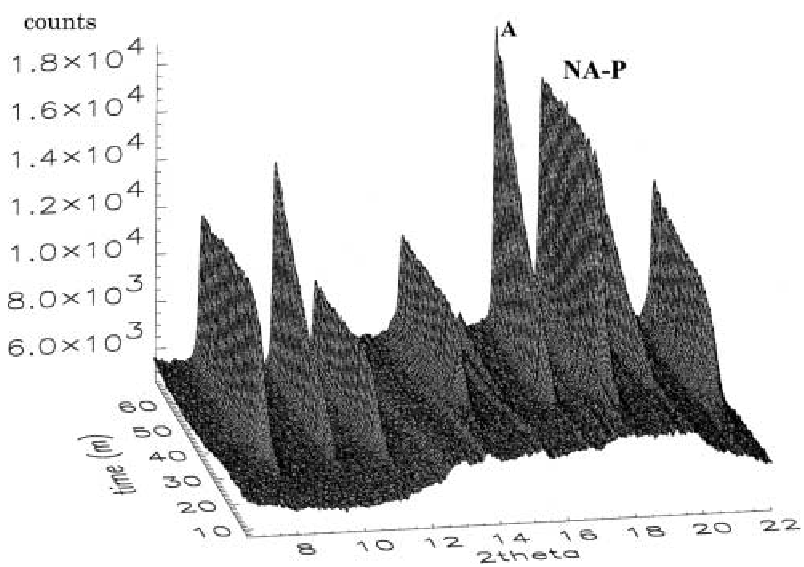

Fig. 1 Three-dimensional plot, 2θ-intensity time of the synthesis of Na-P (*N*) and analcime (*A*) in the isothermal run at 140 °C

Table 1 Reflections used in the integration procedure for each zeolite phase

Na-X S.G. Fd $\bar{3}$m and a = 25.028 Å	Na-P S.G. $C2/c$ a = 14.1324(18); b = 10.0357(12); c = 10.0649(13) Å[a]	Analcime S.G. Ia $\bar{3}$d and a = 13.73 Å
(1 1 0)	(1 1 $\bar{1}$)+(1 1 0)	(2 1 1)
(2 2 0)	(2 0 $\bar{2}$)+(0 2 0)+(2 0 0)	(2 2 0)
(3 1 1)	(1 1 $\bar{2}$)+(1 1 1)+(0 2 1)+ (2 2 $\bar{1}$)+(3 1 $\bar{2}$)+(3 1 $\bar{1}$)	(4 0 0)
(3 3 1)	(0 0 2)+(2 2 $\bar{2}$)+(2 2 0)+(4 0 $\bar{2}$)	(3 3 2)
(5 3 3)	(4 2 0)	(4 3 1)

[a] Refined values

holder with Ag paste, dried using an IR lamp, and coated using a 10-nm gold layer. The instrument was utilized with a vacuum of ca. 10^{-7} torr. The frames were collected using a beam size of 5 μm and an intensity of 25 kV. Point analyses collected on C-coated sample in energy-dispersive mode (EDS) also confirmed the Si/Al ratio and the Na content.

Kinetic analysis

A model to study the reaction kinetics of zeolite nucleation and growth by real-time X-ray powder diffraction has been elaborated. Some basic assumptions have been considered:

1. The crystal growth is not constant. It is constant at constant supersaturation and decreases at the end of the crystallization process as a consequence of the decrease in supersaturation due to the increase in the consumption of reactive species from the liquid phase (increase in mass and surface area of the crystalline phase) and simultaneous decrease in their formation by dissolution of precursor (decrease in the mass and surface area of the precursor).
2. The crystal growth may take place in n dimensions ($n = 1$, monodimensional; $n = 2$, bidimensional; $n = 3$, 3-dimensional) (Bamford and Tipper 1980).
3. The growth symmetry is inferred from the SEM images (crystal morphology) and imposed by crystal symmetry restraints.
4. Nucleation can be homogeneous, heterogeneous or autocatalytic in clear solutions. It can be heterogeneous or autocatalytic in dense solutions.

A general kinetic equation should consider either the nucleation and growth mechanisms in order to fit the sigmoidal α/time plots from $t = 0$ to $t = \infty$:

$$\alpha = \int_0^\infty F_g(t, t_j) F_n \left(\frac{dN}{dt}\right)_{t=t_j} dt_j \ , \tag{1}$$

where F_g = growth expression, F_n = nucleation expression. If we consider an expression for nucleation which effectively takes into account the probability that a number N of nuclei develop at time t, the expression is:

$$P_N = \frac{dN}{dt} = \exp\left\{-\frac{(t-a)^2}{2b^2}\right\} \ . \tag{2}$$

The simple Gaussian distribution of probability described in Eq. (2) accomplishes a = position of the top of the Gaussian peak which is in terms of nucleation, the maximum rate of nucleation; b = the variance of the peak which defines the distribution of the probability of nucleation with time (fundamental to assess the nucleation mechanism). Narrow probability peaks correspond to heterogeneous reactions, large peaks correspond to autocatalytic reactions [the nucleation rate increases during the crystallisation process (Subotić and Graovac 1985)].

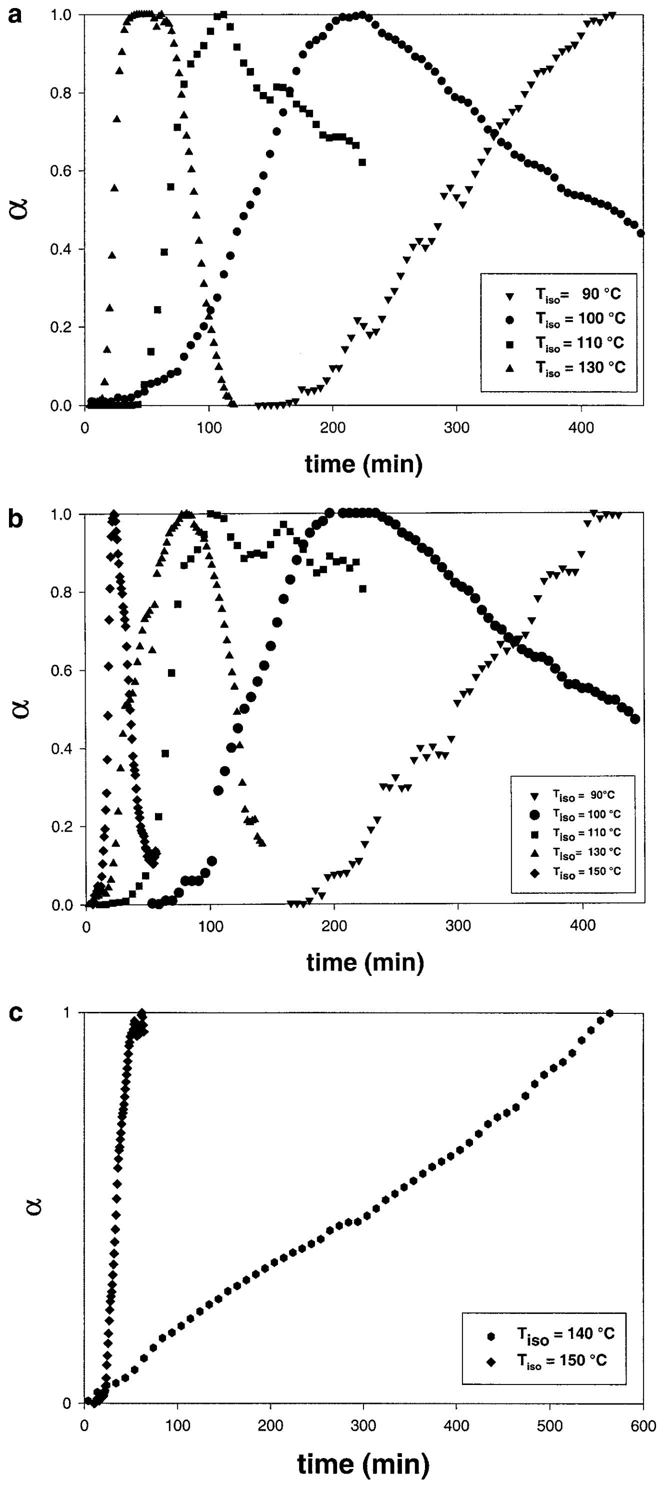

Fig. 2a–c α/time curves for the crystallisation of Na-X (**a**), Na-P (**b**) and analcime (**c**), respectively

A simplified form of Eq. (1) which considers the mass m_s or fraction α of crystalline phase formed in any crystallisation time t_c may be expressed as (Randolph and Larson 1971):

$$\alpha = G \times \sigma \times \int_0^L [L(\tau, t_c)]^n (dN/dL) dL \ , \tag{3}$$

where $L(\tau, t_c)$ is crystal size which depends on the time τ in which the nucleus is formed and time of crystalline t_c, $\mathrm{d}N/\mathrm{d}L$ is particle (crystal) size distribution in time t_c, G is geometrical factor of crystal shape, σ is density of the crystallized solid phase, and $n = 1$ for one-dimensional growth (needles, rods), $n = 2$ for two-dimensional growth (plates) and $n = 3$ for three-dimensional growth (most common case for the growth of zeolites). Assuming a three-dimensional crystal growth ($n = 3$), a combination of Eqs. (2) and (3) gives:

$$\alpha = G \times \sigma \times \int_0^{t_c} [L(\tau, t_c)]^3 \exp\left\{\frac{(\tau - a)^2}{2b^2}\right\} \mathrm{d}\tau \ . \quad (4)$$

The normal (cumulative) expression of the probability function actually yields the total number of nuclei N. Such an expression (of course, sigmoidal) is:

$$N = \frac{1}{1 + \exp\left\{-\left(\frac{t-a}{b}\right)\right\}} \quad (5)$$

The rate constant of nucleation is $k_n = 1/a$. Equation (5) represents the number of nuclei invisible to diffraction. In fact, diffraction can only monitor α, the convolution of the nucleation (N) and crystal growth x. The simple Gaussian expression may be substituted by a more complex function such as a pseudo-Voigt, a Pearson VII or others to empirically reproduce the non-asymmetrical component of the nucleation probability profile. The asymmetry component in the nucleation curves, which is more or less always there, may stem from secondary or multiple nucleation, i.e. a convolution of a number of Gaussian nucleation peaks. For the sake of simplicity, a Gaussian expression integrated with a growth expression is assumed. A valid expression for the growth process is:

$$x = 1 - \exp[-(k_g t)^n] \ , \quad (6)$$

with k_g = rate constant for growth, which is derived from the Kholmogorov equation (Katovic et al. 1989a; Lechert 1996):

$$-[\ln(1 - x)]^{1/n} = k_g t \ , \quad (7)$$

where x = number of diffraction visible crystals, formed from the diffraction invisible nuclei. Here, the parameter n represents the dimension of the growth = 1, 2, 3 and $k = k_g$. Thus, the final kinetic equation monitored by XRD, which includes the nucleation and the growth term ($\alpha = N \cdot x$), is:

$$\alpha = \frac{1}{1 + \exp\left\{-\left(\frac{t-a}{b}\right)\right\}} \cdot \left\{1 - \exp\left[-(k_g t)^n\right]\right\} \quad (8)$$

Fitting a kinetic curve with this expression yields the parametrization of a, b, k_g (growth rate constant) and indirectly the nucleation rate constant, $k_n = 1/a$. a and b in turn can be used to calculate P_N. It is possible to compare the b values with the q values obtained using the approximation (Katović et al. 1989a, b):

$$\alpha = kt^q \ . \quad (9)$$

According to this simple equation, when $q = 3$, the nucleation is heterogeneous, when $q = 4$, the nucleation is homogeneous and when $q > 4$, the nucleation is autocatalytic. A set of q values ranging from 3.9 to 5.5 taken from Gualtieri et al. (1997a) describing the reaction of crystallisation of Na-A zeolite from metakaolinite were considered. Experimental curves originally fitted using Eq. (9) have been refitted using Eq. (8). A linear relationship exists between the kinetic order of the mechanism q and b (Fig. 3) indicating that when $b \le 15$, the nucleation is heterogeneous, when $b \approx 20$, the nucleation is homogeneous, and when $b > 20$, the nucleation is autocatalytic. The fit of the kinetic curves was possible using the program SigmaPlot for Windows version 4.01.

The growth expression is similar to the Avrami–Erofeev equation, a general empirical expression which originates from the Avrami–Mehl–Johnson equation developed for solid-state transformations,

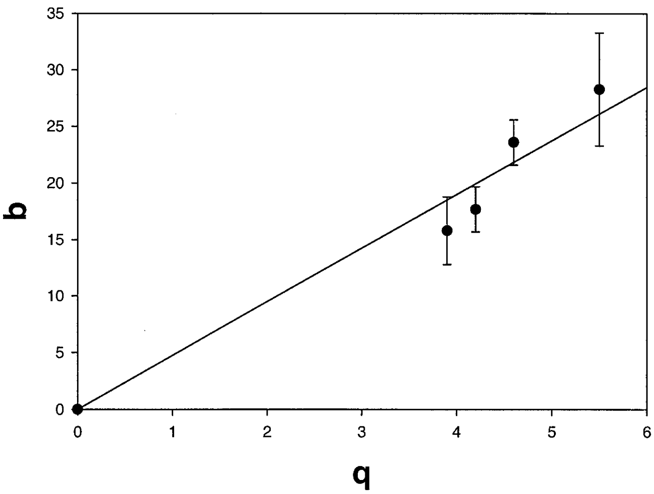

Fig. 3 Linear relationship between the kinetic order of the mechanism q and b calculated using a set of q values ranging from 3.9 to 5.5 for the reaction of crystallisation of Na-A from metakaolinite fitted using equation $\alpha = kt^q$ and refitted here using Eq. (8) (see text for details)

$$\mathrm{d}m_s/\mathrm{d}\tau = k_n \times (m_s^{\mathrm{o}} - m_s) \times \left[k_g \times (t_c - \tau)\right]^3 \ , \quad (10)$$

and hence,

$$\alpha_s = m_s/m_s^{\mathrm{o}} = 1 - \exp\left[-K \times (t_c)^4\right] \quad (11)$$

Here, m_s is the mass of the crystalline phase (e.g. zeolite) formed at time t_c, m_s^{o} is the mass of precursor (e.g. amorphous gel or unstable type of zeolite), k_n and k_g are rate constants of "homogeneous" nucleation and crystal growth, respectively, and $K = [k_n \times (k_g)^3]/4$. It is evident that the rate of nucleation, $R_n = k_n \times (m_s^{\mathrm{o}} - m_s)$is proportional to the amount $(m_s^{\mathrm{o}} - m_s)$ of untransformed precursor, and that both nucleation and linear, time-independent crystal growth occur inside the precursor particles (solid-state mechanism). For a heterogeneous nucleation (growth of a constant number of nuclei present in the precursor), the power in Eq. (10) is 3. On the other hand, it is well known that zeolite crystals cannot grow inside the gel matrix, but only in full contact with the liquid phase, where,

$$\mathrm{d}L/\mathrm{d}t_c = k_g \times [C_{\mathrm{Al}} - C_{\mathrm{Al}}(\mathrm{eq})][C_{\mathrm{Si}} - C_{\mathrm{Si}}(\mathrm{eq})]^n = k_g \times f(C) \quad (12)$$

where C_{Al} and C_{Si} are concentrations of aluminium and silicon in the liquid phase at crystallisation time t_c, C_{Al}(eq) and C_{Si}(eq) are concentrations of aluminium and silicon which correspond to solubility of zeolite at given crystallisation conditions, n is a factor related to the Si/Al ratio in the crystallized zeolite, and $f(C) = [C_{\mathrm{Al}} - C_{\mathrm{Al}}(\mathrm{eq})][C_{\mathrm{Si}} - C_{\mathrm{Si}}(\mathrm{eq})]^n$ is the concentration factor (Bosnar and Subotić 1999; Bosnar et al. 1999). Hence,

$$L = \int_0^{t_c} f(C)\mathrm{d}t_d \ . \quad (13)$$

Although valid only for solid-state reactions and not for solution-mediated processes, the Avrami expression has been used in the past with some success for the description of growth kinetics of zeolites (Norby 1997; Di Renzo et al. 1991; Mintova et al. 1992). The main concern in its application to solution-mediated processes is the physical meaning of the parameter n, which empirically refers to nucleation and growth mechanisms valid for solid-state reactions. Here, n has a strict meaning as it refers to the growth dimension (1, 2, 3) rigorously restrained by the crystal symmetry (a needle-like fibrous morphology indicates a mono-dimensional growth, a platelet-like morphology indicates a two-dimensional growth, and a cube-like or an isotropic morphology addresses a three-dimensional growth).

Growth curves vs. time were calculated from the real-time data for each zeolite phase since the observed FWHM can be empirically correlated to the size of coherent domains D(Å) throughout the Scherrer equation $D = K \cdot \lambda / (\beta \cos \theta)$ (Jenkins 1989). The FWHM should be corrected for the instrumental broadening to obtain absolute values of βs. Since for the correlation curves, absolute values are not required, the instrumental correction was not performed and FWHM vs. time was extracted for the (1 1 1) reflection of Na-X, (0 0 2) and (3 0 1) reflections of Na-P and (4 0 0) reflection of analcime, respectively.

Results

Na-X [$Na_{88}(Si_{104}Al_{88}O_{384})\cdot 220H_2O$, Si/Al = 1.18 from the chemical analysis] and Na-P [$Na_{74.8}(Si_{117.2}Al_{74.8}O_{384})\cdot 171.7H_2O$, Si/Al = 1.57 as calculated from the structure refinement] co-crystallise in the temperature range 90–130 °C. At higher temperatures and for longer times, Na-X is unstable and transforms into Na-P (Fig. 4a) in the range 130–150 °C. Na-P, in turn, transforms (Fig. 4b) into analcime [$Na_{16}(Si_{32}Al_{16}O_{96})\cdot 16H_2O$, Si/Al = 2] at 140 and 150 °C. Figure 5 shows the co-crystallisation curves and relative conversions of Na-X to Na-P at 90 °C (Fig. 5a) and 130 °C (Fig. 5b) and Na-P to analcime at 150 °C (Fig. 5c), respectively. The formation of Na-X and Na-P are competitive processes: Na-X seems to have a much faster crystallisation than Na-P which, in turn, does not form at the expense of Na-X but directly from the dense solution. In fact, when metastable Na-X starts to dissolve, Na-P is more or less completely crystallised. The scenario changes for the Na-P to analcime conversion because analcime clearly forms at the expense of Na-P.

The refined structure of Na-P was not reported here, since it is basically identical to that of Albert et al. (1998) with space group *C2/c* and refined cell reported in Table 1. The structure details and full dataset are available upon request from the author.

Figure 6 reports an example of the crystallisation curves with relative curve fit using Eq. (7), and calculated nucleation curves using Eq. (2), of the zeolite Na-X at 100 °C. The extracted values of the nucleation and growth-rate constants (k_n and k_g, respectively), the

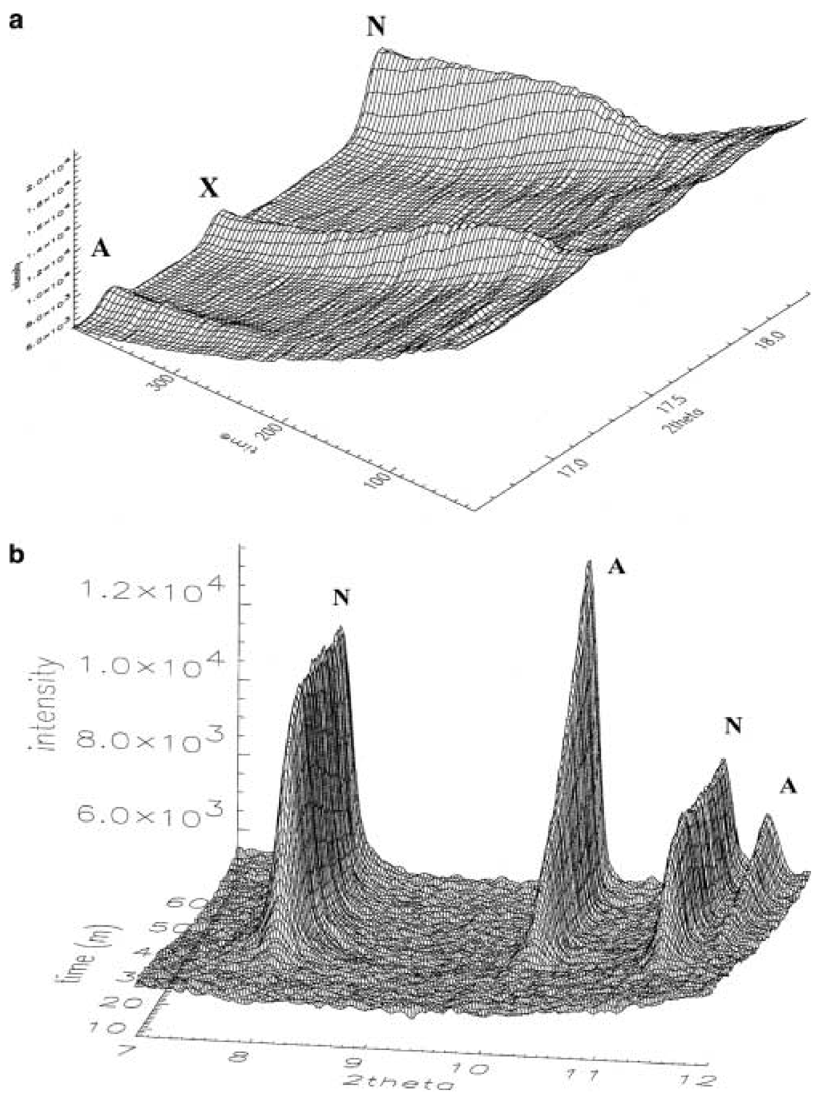

Fig. 4 Selected three-dimensional plot, 2θ-intensity time of the Na-X (X) and Na-P (N) cocrystallisation at the isothermal run at 130 °C and Na-P (N) to analcime (A) transformation in the isothermal run at 140 °C

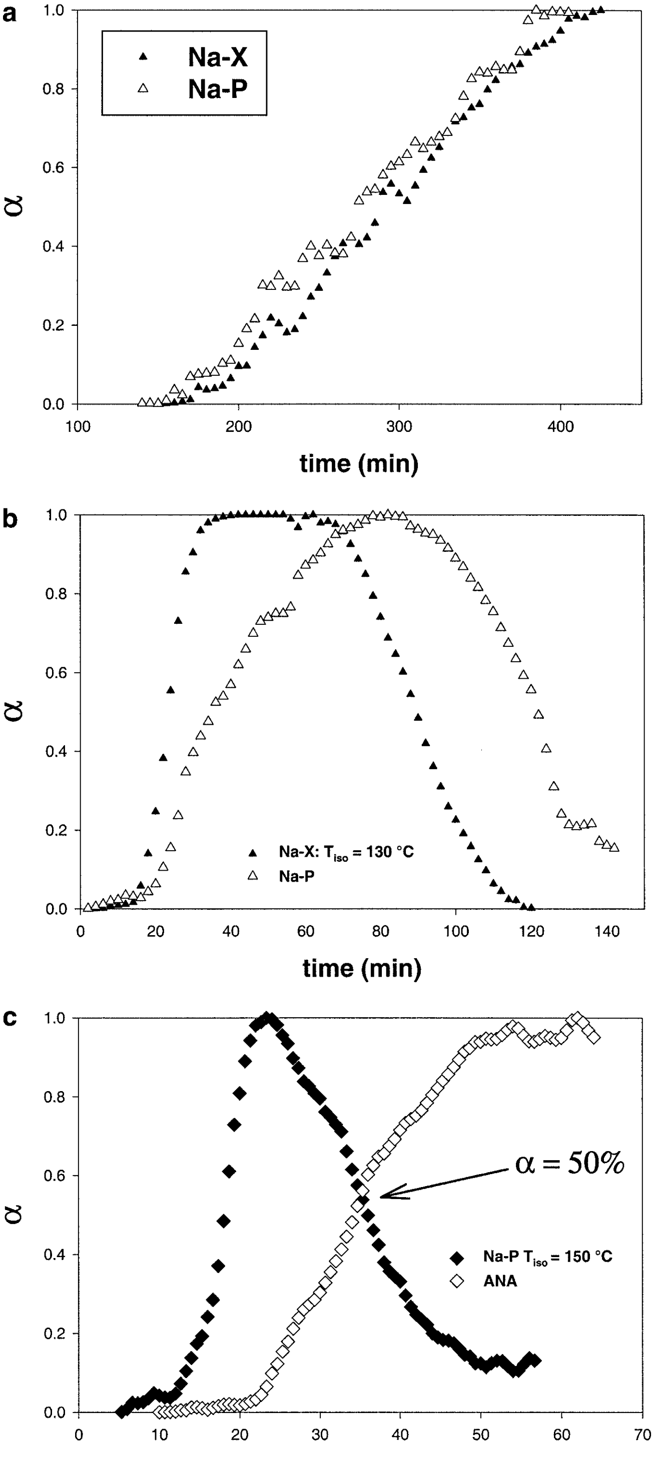

Fig. 5a–c Selected two-dimensional cocrystallisation curves of Na-X to Na-P at 90 °C (**a**) and 130 °C (**b**) and of Na-P to analcime at 150 °C (**c**)

coefficient of distribution of the probability of nucleation b, and the coefficient indicating the maximum rate of nucleation a, are reported in Table 2. For Na-X and Na-P it was possible to calculate the apparent activation energy for the nucleation ($E_{a,n}$) and growth ($E_{a,g}$) and

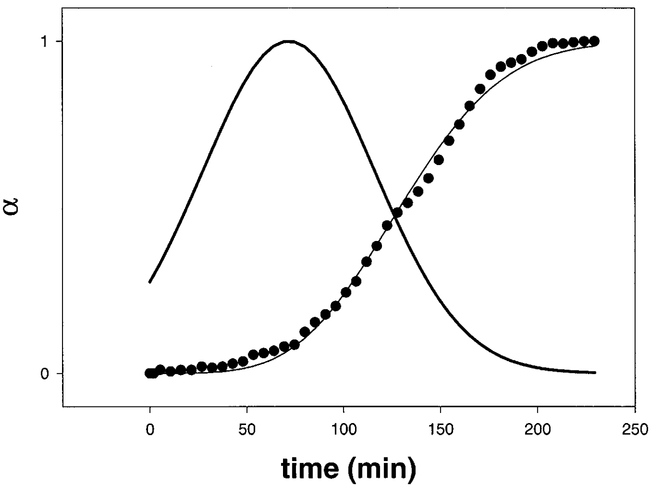

Fig. 6 Examples of crystallisation curves with relative curve fit using Eq. (8) (*full dots* and *thin line*) and calculated nucleation curves (*thick line*) using Eq. (2), of the zeolite Na-X at 100 °C

relative frequency factors using the Arrhenius equation $k = A\ \exp(-E/RT)$ in the logarithmic form $\ln(k)$ vs. $1/T$. Energies are calculated from the slope of the linear plot while the preexponential frequency factors are calculated from the constant term (Fig. 7). The results of the kinetic analysis are also reported in Table 2. The regression coefficients R^2 were close to 0.990. Only the R^2 of the Arrhenius plot of the Na-P nucleation and growth were 0.97 and 0.93, respectively.

Examples of plots of FWHMs (°2θ) vs. time are reported in Fig. 8a, b, c for the three zeolite phases. They all are linear, indicating that the crystal growth rate is constant in the early stages of the crystallisation reaction.

The SEM pictures of the Na-P zeolite formed at 130 °C show that at lower magnification (Fig. 9a) the shape of the crystals is apparently spherulitic (as already described in Katović et al. 1989a, b). Spherulites have a diameter of about 1 μm and are actually aggregates of platelets or platy crystals (Fig. 9b), indicating the presence of twinning and that the symmetry of Na-P is obviously lower than cubic.

Discussion

The environment of formation of the zeolites is a dense solution of NaOH, water and a gel precursor that can be considered a non-homogeneous monophasic gel with a three-dimensional random network of SiO_2 and Al_2O_3 coordination polyhedra (dehydroxylated halloysite = DH) intermixed at an atomic scale with islands of SiO_2-rich regions (amorphous silica = AS). At lower isothermal temperatures Na-X and Na-P cocrystallize (Fig. 5a). Na-X tends to dissolve earlier than Na-P (Fig. 5b) which, in turn, transforms into analcime (Fig. 5c). For both zeolites, the coefficient b of Eq. (7) indicates an autocatalytic nucleation (Table 2) at lower isothermal temperatures and a heterogeneous nucleation

Table 2 Results of the kinetic analysis

Isotherms (°C)	a (min)	b	k_n	k_g	$E_{a,n}$ (kcal mol^{-1})	$E_{a,g}$ (kcal mol^{-1})	A_n (min^{-1})	A_g (min^{-1})
Na-X								
90	120 (50)	24 (3)	0.0083 (2)	0.0029 (1)				
100	72 (25)	32 (9)	0.0139 (2)	0.0067 (1)				
110	59 (3)	6.6 (5)	0.0169 (4)	0.0153 (3)				
130	33 (1)	2.8 (1)	0.0303 (2)	0.08 (1)				
					9 (2)	24 (1)	1.0 (1) × 10^5	1.5 (1) × 10^{10}
Na-P								
90	350 (24)	24 (4)	0.0028 (3)	0.0028 (1)				
100	188 (11)	15 (2)	0.0053 (3)	0.0073 (2)				
110	95 (20)	4.7 (9)	0.010 (9)	0.0157 (5)				
130	62 (2)	2.2 (2)	0.016 (1)	0.0440 (9)				
150	20 (2)	1.5 (3)	0.05 (1)	0.059 (6)				
					13 (1)	16 (1)	6.0 (1) × 10^5	3.0 (2) × 10^6
Analcime								
140	373 (58)	27 (8)	0.0019 (3)	0.08 (1)				
150	15 (1)	21 (5)	0.069 (1)	0.025 (3)	–	–	–	–

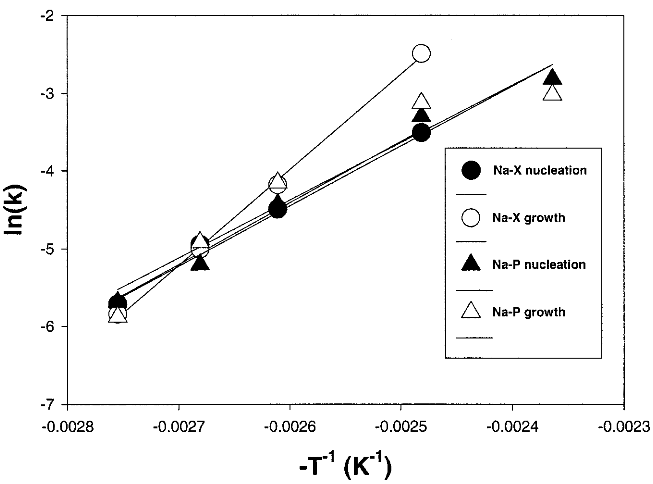

Fig. 7 Arrhenius plots for the calculation of the apparent activation energy for the nucleation ($E_{a,n}$) and growth ($E_{a,g}$) reactions and relative frequency factors of Na-X (**a**) and Na-P (**b**) zeolites

at higher isothermal temperatures with a constant crystal growth (Fig. 8a, b) in 3-D for Na-X and 2-D growth for Na-P, respectively. Random autocatalytic nucleation occurs within the gel regions or at the interface gel–solution at an explosive rate. It is possible to speculate that most aluminous Na-X nucleates mainly within the DH regions and most siliceous Na-P nucleates mainly at the interface between the DH and the AS regions. Since $k_n > k_g$, the rate-limiting step must be the crystal growth. At isothermal temperatures higher than 100 °C for Na-P and 110 °C for Na-X, respectively, b drops, indicating that nucleation becomes heterogeneous and takes place only at the interface gel–solution. The rate-limiting step is then the nucleation itself, since $k_n < k_g$. The fast crystal growth (the solution is supersaturated) determines a fast consumption of all possible sites for nucleation and prevents autocatalysis. The point at 150 °C for Na-P is anomalous, since $k_n > k_g$.

The autocatalytic model for Na-P is in agreement with the early observation reported in of Katović et al. (1989a, b), indicating an increasing crystallisation rate of Na-P(t) as a consequence of autocatalytic nucleation and linear, time-independent growth.

At higher temperatures, Na-P is more stable than Na-X as the latter is dissolved much faster. Usually, the transformation of the metastable zeolite into a more stable phase takes place according to the Ostwald rule of successive transformations and the nucleation and crystallisation of the new phase occur in the supersaturated solution throughout the dissolution of the former phase. Since Al···Al interaction energy of the faujasite-like structures is considerably higher than Al···Al interaction energy of zeolite P (Shuije et al. 1985), Na-X is the unstable phase with respect to zeolite Na-P, and the transformation of amorphous gel into Na-X and the transformation of X into zeolite Na-P are spontaneous processes (Katović et al. 1989a, b). The most porous zeolites such as Na-X with pore volumes in the range 0.45–0.53 cm^{-3} of crystal do not form at temperatures above 100 °C. A consequence of the decrease in intracrystalline porosity is the change in the Si/Al ratio of the zeolite formed at higher temperature. In fact, we observe that the Si/Al ratio increases from NaX to analcime (from 1.18 to 2) with temperature/time. A large Si/Al ratio requires a lower number of extraframework cations, and consequently the framework density increases as revealed by a linear relationship ($R^2 = 0.999$) between Si/Al and framework density (T 1000 Å^{-3}) of the forming zeolites (12.7 vs. 1.18, 15.4 vs. 1.57 and 18.6 vs. 2.00). A similar result was described by Drag et al. (1985) for Na-X and Na-Y. Moreover, the activation energy of crystallisation is also a function of the Si/Al ratio: the more silicious the zeolite, the larger the activation energy (Kacirek and Lechert 1976). Barrer (1982) observed that for zeolite Na-Y, the larger the Si/Al ratio in the crystals formed, the larger the activation energy (from Si/Al = 1.53 and $E_a = 11.8$ kcal mol^{-1} to Si/

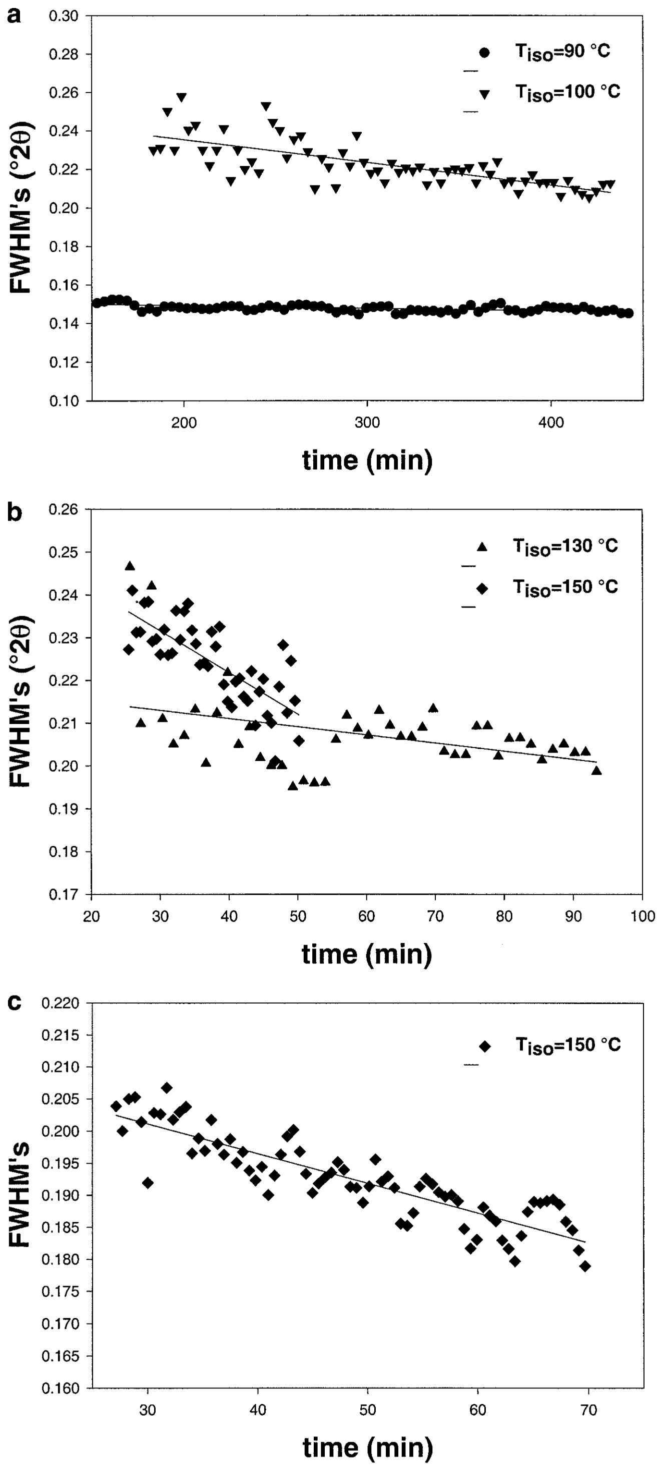

Fig. 8a–c Examples of plots of D (Å) vs. time for Na-X (**a**), Na-P (**b**) and analcime (**c**), indicating a constant crystal growth rate

$Al = 2.54$ and $E_a = 15.6$ kcal mol^{-1}). The process involves the formation of T–O–Si bonds (T = Al or Si):

$$\equiv T-O^{-}Na^{+} + H-O-Si\equiv \Rightarrow \equiv T-O-Si\equiv + NaOH$$

$$\equiv T-OH + HO-Si\equiv \Rightarrow \equiv T-O-Si\equiv + H_2O$$

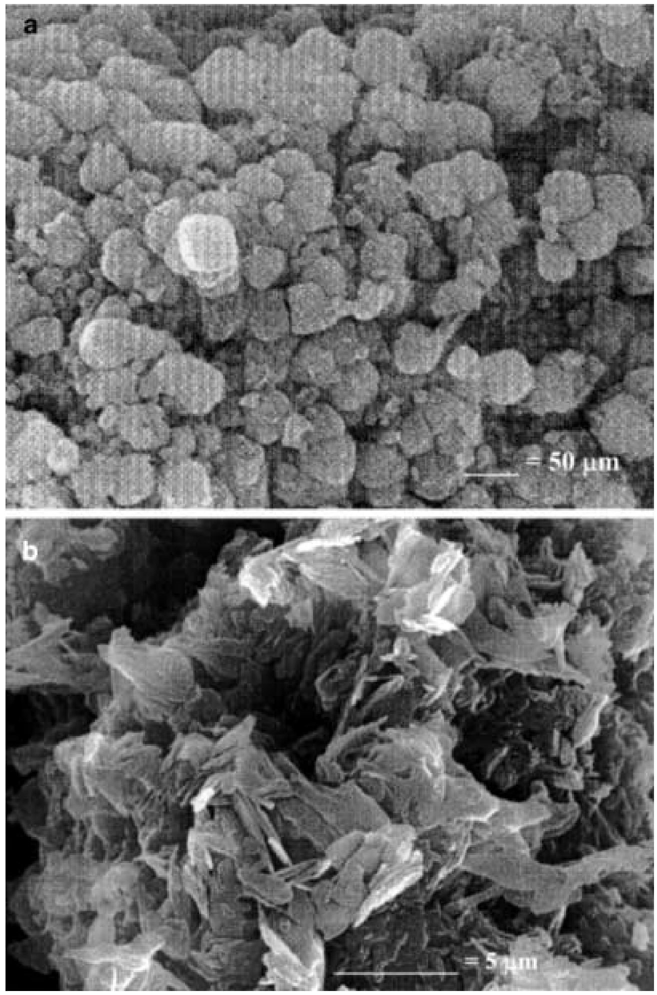

Fig. 9a, b SEM pictures of the Na-P zeolite formed at 130 °C at low magnification (**a**) and at high magnification (**b**)

and the elimination of water or NaOH occurs with a lower activation energy when T = Al than when T = Si. In concert, the activation energy of nucleation of Na-X with Si/Al = 1.18 is lower than the activation energy of nucleation of Na-P with Si/Al = 1.57 (Table 2). Unfortunately, it is not possible to calculate any activation energy for analcime using two isotherms.

Regarding the structure of the Na-P zeolite, it is confirmed here that the symmetry is monoclinic $C2/c$, as already proposed by Albert et al. (1998).

At $T > 140$ °C Na-P is unstable and transforms into analcime. There are many possible transformation mechanisms for zeolites, as quoted in Norby (1997): (1) internal structural transformation; (2) gel-mediated transformation; (3) solution-mediated transformation; (4) surface-mediated transformation; (5) structural similarity enhanced transformation or epitaxial crystallisation.

Figure 10 is a high-magnification SEM image of the reacting phases during the run at 150 °C. Analcime crystals form on the aggregates of dissolving Na-P

Fig. 10 SEM image of the phases in the system during the run at 150 °C

platelets, indicating that no surface-mediated (4) or epitaxial transformation (5) occur, and that a solution-mediated transformation is very likely. Na-P dissolves in solution which is, in turn, readily supersaturated and precipitates analcime. On the other hand, both mechanisms (2) and (3) generally take place through partial or complete transformation of the starting material into an amorphous phase and seem to be ruled out here for the Na-P to analcime transformation since the crystallisation curve of analcime and the degradation curve for Na-P cross close to 50% conversion. In fact, if the starting material had been partly or completely dissolved into amorphous material, the conversion curves would cross below 50% crystallinity. A possible explanation is that all the dissolved phase from Na-P zeolite more or less instantaneously transforms into crystalline analcime phase, i.e. a mass balance of dissolved Na-P and formed analcime is established.

Conclusions

The hydrothermal crystallisation sequence of zeolites formed in the T range 90–150 °C in NaOH solution from an halloysite sample preventively activated at 600 °C shows that at lower isothermal temperatures Na-X and Na-P co-crystallize. Na-X tends to dissolve prior to Na-P which, in turn, is converted into analcime. For both Na-X and Na-P zeolites, an autocatalytic nucleation is found at lower isothermal temperatures and an heterogeneous nucleation at higher isothermal temperatures with a constant crystal growth. The structure of the synthesized Na-P has a monoclinic symmetry. At $T > 140$ °C Na-P is unstable and transforms into analcime probably throughout a solution-mediated transformation.

Finally, it should be remarked that natural halloysite can be a very good precursor for the synthesis of zeolites and especially Na-P zeolite at temperatures around 130 °C.

Acknowledgements This research is supported under contract DE-AC02-98CH10886 with the US Department of Energy, by the Division of Chemical Sciences, Office of Basic Energy Sciences. This work is also part of a project entitled Growth of Zeolites in Microgravity financed by the ASI and ESA. G. Artioli and P. Norby are kindly acknowledged for help in the experimental part, useful discussions and reading of the manuscript. B. Subotić is greatly acknowledged for his patience in exchanging ideas with a stubborn mineralogist, critical improvement of the manuscript, and fruitful "never-ending" discussion and criticism.

References

Albert BR, Cheetham AK, Stuart JA, Adams CJ (1998) Investigations on P-zeolites: synthesis and structure of the gismondine analogue, highly crystalline low-silica NaP. Micropor Mesopor Mat 21(1–3): 133–142

Amemija Y (1990) Imaging plate – X-ray area detector based on photostimulable phosphor. Synchr Rad News 3: 21–26

Bailey SW (1988) In: Hydrous phyllosilicates. Reviews in Mineralogy, vol 19, Mineralogical Society. America, Washington, DC

Bamford CH, Tipper CHF (1980) Comprehensive chemical kinetics. Elsevier. New York

Barrer RM (1982) Hydrothermal chemistry of zeolites. Academic Press, New York

Barrer RM, Mainwaring DE (1972) Chemistry of soil minerals. Part XIII. Reactions of metakaolinite with single and mixed bases. J Chem Soc Dalton: 2534–2546

Barrer RM, Cole JF, Sticher H (1968) Chemistry of soil minerals: Part V. Low-temperature hydrothermal transformations of kaolinite. J Chem Soc Dalton: 2475–2485

Bosnar S, Subotić B (1999) Mechanism and kinetics of the growth of zeolite micro-crystals. Part 1: influence of the alkalinity of the system on the growth kinetics of zeolite A microcrystals. Micro Meso Mat 28: 483–493

Bosnar S, Bronic J, Subotić B (1999) Analysis of the influence of kinetic and chemical factors on the rate of crystal growth of zeolite A. In: Kiricsi L, Pal-Borbely G, Nagy JB, Karge HG (eds) Porous materials in environmentally friendly processes. Proceedings of the 1st International FEZA Conference Stud Surf Sci Catal 125: 69–76

Breck DW (1974) Zeolite molecular sieves. J Wiley, New York

Costanzo PM, Giese RF (1985) Dehydration of synthetic hydrated kaolinites: a model for the dehydration of halloysite (10 Å). Clays Clay Miner 33: 415–422

Di Renzo F, Remouè F, Massiani P, Fajula F, Figueras F (1991) Crystallization kinetics of zeolite TON. Zeolites 11: 539–548

Drag EB, Miecznikowski A, Abo-Lemon F, Rutkowsi M (1985) Synthesis of A, X and Y zeolites from clay minerals. In: Drzai B, Hocevar S, Pejovnik S (eds) Zeolites. Elsevier, New York, 147 p

Gualtieri AF, Bertolani M (1991a) Ceramic raw materials in the Viterbo district. In: Vincenzini P (ed) Ceramics today – tomorrow's ceramics. Elsevier, B. V. New York, pp. 119–128

Gualtieri AF, Bertolani M (1991b) Materie prime di interesse ceramico nella Provincia di Viterbo (Italia Centrale). Ceramurgia 2: 63–67

Gualtieri AF, Norby P (1998) Kinetics of hydrothermal synthesis of Li-ABW from metakaolinite by time-resolved synchrotron diffraction. Mat Sci Forum 278–281: 418–423

Gualtieri AF, Norby P, Artioli G, Hanson J (1997a) Kinetics of formation of zeolite Na-A [LTA] from natural kaolinites. Phys Chem Miner 24: 191–199

Gualtieri AF, Norby P, Artioli G, Hanson J (1997b) Kinetic study of hydroxysodalite formation from natural kaolinites by time-resolved synchrotron powder diffraction. Micro Mat 9: 189–201

Hastings JB, Suortii P, Thomlinson P, Kvick Å, Koetzle T (1990) Optical design for the NSLS crystallography beamline. Nucl Instr Meth 208: 55–58

Jenkins R (1989) Experimental procedures. In: Modern powder diffraction. Reviews in Mineralogy, vol 20, Mineralogical Society America, Washington, DC, pp 48–99

Kacirek H, Lechert HJ (1976) Investigation on the growth of the zeolite type Na Y. J Phys Chem 79: 1589–1593

Katović A, Subotić B, Smit B, Despotović LA (1989a) Crystallization of tetragonal (B8) and cubic (B1) modification of zeolite NaP from freshly prepared gel. Part 1. Mechanism of crystallization. Zeolites 9: 45–53

Katović A, Subotić B, Smit B, Despotović LA (1989b) Crystallization of tetragonal (B8) and cubic (B1) modification of zeolite NaP from freshly prepared gel. Part 2. Kinetics of crystallization. Zeolites 10: 634–641

Larson AC, von Dreele RB (1996) GSAS. Los Alamos Nat Lab, Los Alamos New Mexico 86, LAUR

Lechert H (1996) The mechanism of faujasite growth studied by crystallization kinetics. Zeolites 17: 473–481

Madani A, Aznar A, Sanz J, Serratosa JM (1990) ^{29}Si and ^{27}Al NMR study of zeolite formation from alkali-leached kaolinites. Influence of thermal preactivation. J Phys Chem 94: 760–765

Mintova S, Valtchev V, Vultcheva E, Veleva S (1992) Crystallization kinetics of zeolite ZSM-5. Zeolites 12: 210–215

Norby P (1996) In situ time-resolved synchrotron powder diffraction studies of syntheses and chemical reactions. Mat Sci Forum 147: 228–231

Norby P (1997) Hydrothermal conversion of zeolites: an in situ synchrotron X-ray powder diffraction study. J Am Chem Soc 119: 5215–5222

Randolph DA, Larson MA (1971) Theory of particulate processes. Academic Press, New York, p 20

Rollman LD (1984) In: Ribero FR, Rodrigues AE, Rollman LD, Naccache C (eds) Zeolites: science and technology. Nato ASI Series, Martinus Nijhoff Publishers

Shuije M, Liansheng L, Ruren X, Zhaohui Y (1985) The mechanism of transformation of NaY to NaPc type zeolites. In: Drzai B, Hocevar S, Pejovnik S (eds) Zeolites. Elsevier, New York, pp 191–198

Subotić, B, Graovac A (1985) Kinetic analysis of autocatalytic nucleation during crystallisation of zeolites. In: Drzai B, Hocevar S, Pejovnik S (eds) Zeolites. Elsevier, New York, pp 199–206

Treacy MMJ, Higgins JB, von Ballmoos R (1996) Zeolites, collection of simulated XRD powder patterns for zeolites, 16